

# Contents

<b>1</b>	<b>Introduction</b>	<b>2</b>
<b>2</b>	<b>Theory</b>	<b>2</b>
2.1	Diffraction . . . . .	2
2.2	Aperture Function . . . . .	2
2.3	Amplitude Grating . . . . .	3
2.4	Resolution . . . . .	3
2.5	Phase Grating . . . . .	4
2.6	Raman-Nath-Theory . . . . .	4
<b>3</b>	<b>Experimental Setup</b>	<b>5</b>
<b>4</b>	<b>Execution of the Experiment</b>	<b>6</b>
<b>5</b>	<b>Data Analysis</b>	<b>8</b>
5.1	Grating Constant of a Sine Grating . . . . .	8
5.2	Grating Constants of five Amplitude Gratings . . . . .	9
5.2.1	Angle-Time Calibration . . . . .	9
5.2.2	Grating Constants of the five Amplitude Gratings . . . . .	11
5.2.3	Resolution of five Amplitude Gratings . . . . .	12
5.2.4	Aperture Function of Grating 1 . . . . .	12
5.2.5	Proportion of Slit Width and Grating Constant of Grating 1 . . . . .	14
5.3	Examination of the Phase Grating . . . . .	14
5.4	Comparison to the Raman-Nath-Theory . . . . .	15
5.5	Calculation of the wavelength in isoctane . . . . .	18
<b>6</b>	<b>Summary and Discussion</b>	<b>22</b>
6.1	Sine Grating . . . . .	22
6.2	Amplitude Gratings . . . . .	22
6.3	Phase Gratings . . . . .	23
<b>A</b>	<b>Appendix</b>	<b>25</b>
	List of Figures . . . . .	25
	List of Tables . . . . .	26
	Bibliography . . . . .	26
A.1	Interference Pattern for each Grating . . . . .	28
A.2	Interference Pattern for the Ultrasonic Chamber at different Voltages . . . . .	30
A.3	Lab Notes . . . . .	34

# 1 Introduction

The goal of this experiment is to examine the diffraction of light for different types of diffraction gratings.

First, the light of a laser is passed through amplitude gratings, the observable diffraction patterns are then used to determine the grating constants as well as the resolution. In addition, for one of the amplitude gratings the aperture function and the proportion of slit width and grating constant are calculated.

In the second part of the experiment, a phase grating created by an ultrasonic wave in isooctane is examined. The measurements results are compared to the Raman-Nath-Theory and used to calculate the wavelength of the ultrasonic wave.

## 2 Theory

In this section, an overview of the theoretic background necessary for this experiment is given. Diffraction and aperture functions as well amplitude gratings and phase gratings and their differences will be discussed. If not specified otherwise, the information in this section is taken from the manual [1].

### 2.1 Diffraction

When light encounters an obstacle, its propagation can not fully be described by reflection and refraction. The phenomena of light bending around the corners of an obstacle it encounters is referred to as diffraction. This is most easily described using Huygens principle, which states that every point of a wave is the origin of a spherical wave. The sum of those spherical waves make up the wave front. When a wave encounters an obstacle, every point of the wave front that passes the obstacle creates a spherical wave. These spherical waves then interfere, leading to the observed interference patterns.

### 2.2 Aperture Function

The properties of an object can be described by the aperture function, which maps each point to its transitivity. Using the Fresnel-Kirchhoff integral equation, it is possible to show that the intensity distribution  $I$  on the screen is given by the fourier-transformed of the aperture function  $g(x)$

$$I(x) = \left| \int_{\text{obstacle}} g(\mathbf{k}) e^{i\mathbf{k}\cdot\mathbf{r}} d\mathbf{k} \right|^2. \quad (1)$$

In return, the aperture function can be calculated taking the fourier-transformed of the intensity distribution.

### 2.3 Amplitude Grating

An amplitude grating is an object for which the transitivity depends on the position the light passes through. This leads to a modulation in the amplitude of the light, the refractive index however is constant. An amplitude grating is usually characterized by grating constant  $k$  which describes the distance between grid lines, and the slit width  $b$ .

The angle  $\varphi$ , at which an intensity maximum of order  $m \in \mathbb{Z}$  is observed, can be calculated using the wave length of the light  $\lambda$  and the grating constant  $k$  by

$$\sin \varphi = \frac{m\lambda}{k}. \quad (2)$$

The aperture function  $g(x)$  of an amplitude grating is a rectangle function of period  $k$  with a rectangle width of  $b$ . The height of the rectangle is 1, corresponding to a transitivity of 100%. It is also possible to calculate the aperture function using the intensity distribution. This can be done by approximating the fourier-transformed with a fourier-series

$$g(x) = \sum_{j=0}^{\infty} \pm \sqrt{I_j} \cdot \cos 2\pi j \frac{x}{k}, \quad (3)$$

where  $I_j$  is the intensity of the  $j$ -th interference maximum.

For a sine grating, which has a periodic transitivity, the aperture function for first-order maxima is approximately given by

$$g(x) = \sqrt{I_0} + \sqrt{I_1} \cdot \cos 2\pi \frac{x}{k}. \quad (4)$$

### 2.4 Resolution

In general, the resolution of a grating is defined by

$$a = \frac{\lambda}{\Delta\lambda}, \quad (5)$$

where  $\lambda$  is the wave length of the light, and  $\Delta\lambda$  is the minimal difference in wave length for which the intensity maxima are distinguishable.

It can also be calculated from the number of illuminated grid lines  $N$  and the highest order  $m_{\max}$ , for which the maximum can be observed using

$$a = N \cdot m_{\max}. \quad (6)$$

In this experiment,  $N$  is calculated from the beam width  $d$  and the grating constant  $k$

$$N = \frac{d}{k}. \quad (7)$$

## 2.5 Phase Grating

A phase grating is a grating for which the transitivity is constant, but the index of refraction varies in space. As a higher index of refraction corresponds to a lower speed of light, this leads to a local difference in the optical path length (OPL) of the light, which causes diffraction.

In this experiment, the phase grating is realized by an ultrasonic wave in isooctane. Inside the ultrasonic chamber, two quartz crystals are placed inside liquid isooctane ([2], page 22). By applying an alternating voltage with a certain frequency  $\nu$  to the crystals, they produce density-fluctuations in the isooctane which lead to locally different refractive indices. As the difference in the refractive index  $\Delta n$  is proportional to the difference in density  $\Delta\rho$

$$\frac{\Delta n}{n-1} = \frac{\Delta\rho}{\rho}, \quad (8)$$

the ultrasonic wave causes periodic fluctuations in the density of the isooctane, which corresponds to fluctuations in the refractive index.

For an ultrasonic wave length of  $\Lambda$ , the refractive index  $n$  in the liquid is described by

$$n(x) = n_0 + \sin \frac{2\pi x}{\Lambda}. \quad (9)$$

## 2.6 Raman-Nath-Theory

The Raman-Nath-Theory states that the angle  $\varphi$  at which an interference maximum of order  $m$  occurs can be calculated from the wave length of the light  $\lambda$  and the ultrasonic wave length  $\Lambda$  and is given by

$$\sin \varphi = \frac{\lambda}{\Lambda} m \quad (10)$$

It also provides the following connection of the intensity of interference maxima  $I_m$  of order  $m$  and Bessel functions  $J_m$  of order  $m$

$$I_m = J_m^2 \left( \frac{2\pi D \Delta n}{\lambda} \right) = J_m^2(\alpha U_{\text{US}}). \quad (11)$$

Here,  $D$  is the width of the phase grating medium and  $U_{\text{US}}$  the voltage applied to the crystal producing the ultrasonic wave, which is proportional to the difference  $\Delta n$  in the refractive index.

### 3 Experimental Setup

A schematic structure of the setup used for the experiment is visible in [fig. 1](#).

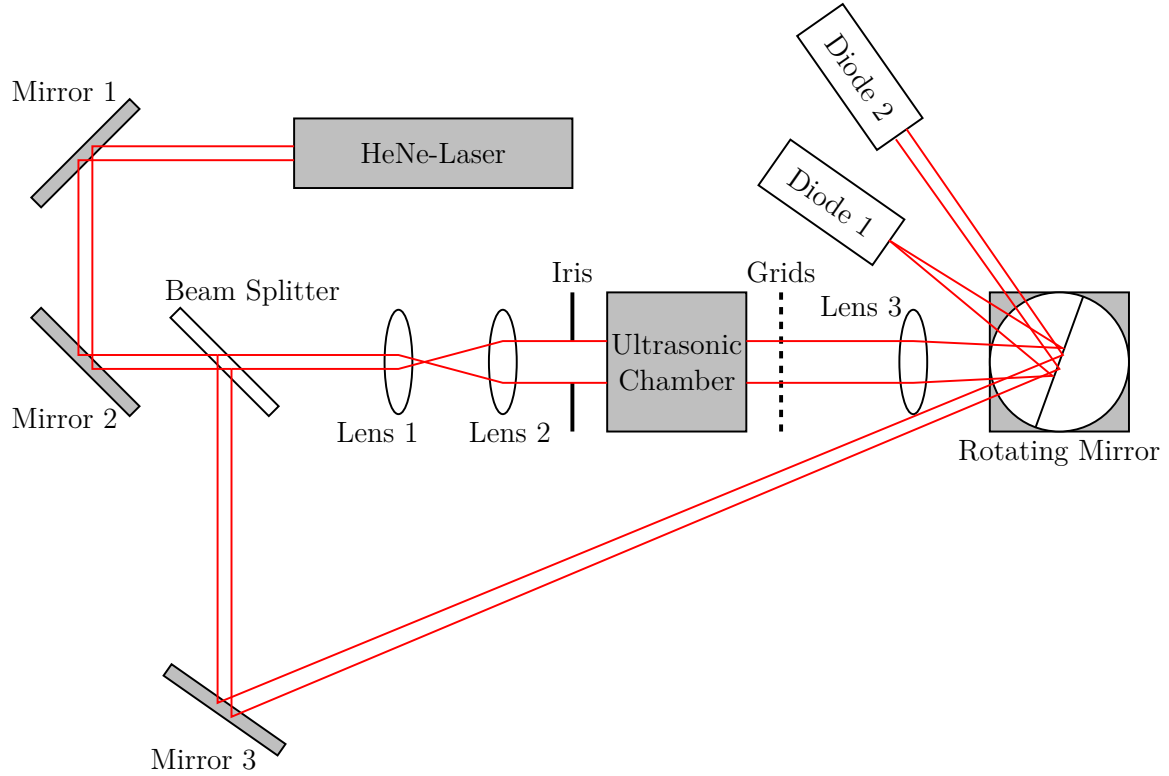


**Figure 1:** Schematic structure of the used setup. The ultrasonic chamber was controlled by a transmitter providing a given frequency and amplitude. The output of the two diodes was amplified and shown on an oscilloscope where diode 2 was used as the trigger signal and diode 1 for the measurement. The focal lengths of the lenses are the following: Lens 1:  $f_1 = 50$  mm, Lens 2:  $f_2 = 100$  mm, Lens 3:  $f_3 = 300$  mm.

To perform the measurements, a continuous light beam with well known wave length is necessary. This is realized using a HeNe-Laser (Helium-Neon-Laser) as it is known for its high purity of the emitted spectrum. The wave length of the emitted light is constant at  $\lambda = 632.8$  nm. Using the mirrors 1 and 2, the light beam is directed onto the optical axis. After passing a beam splitter, the light reaches lenses 1 and 2. These are used to widen the beam profile. It is important that the light after both lenses is collimated again to ensure that only the diffraction at the gratings and not the widening of the light beam is measured. To guarantee this, the distance of both lenses must equal the sum of both focal lengths. The focal lengths of the lenses are  $f_1 = 50$  mm,  $f_2 = 100$  mm. Directly behind the lenses, an iris is used to assure a clean beam profile at the edges.

In the first part of the experiment, a sine amplitude grating is examined. To do so, the grating is placed behind lens 2 and the interference pattern is displayed on a screen added to the optical axis after the grating.

After the sine grating a reference grating with known groove density ( $g_{\text{ref}} = 80 \text{ L/cm}$ ) and 5 other amplitude gratings are examined. Therefore, the setup from [fig. 1](#) is used without the ultrasonic chamber and lens 3. The gratings are again positioned directly behind the iris. After passing the gratings, the light beam hits the rotating mirror and is reflected to diode 1, which can now scan the signal with a time delay due to the rotation of the mirror. Diode 2 is used as a trigger signal to determine the maximum peak position. To do so, the light beam has been split and redirected by mirror 3 towards the rotating mirror where it is redirected to diode 2.

With this setup it is possible to scan a wide range of the interference patterns of the different gratings. The signals of both diodes are amplified using an amplifier-unit and the signal of diode 1 is shown on an oscilloscope, using diode 2 as trigger signal.

For the second part of the experiment, the ultrasonic chamber is placed on the optical axis, behind the iris. It is used as a phase grating. The quartz crystals are controlled by an ultrasound transmitter providing a given frequency  $\nu$  and voltage amplitude  $U_{\text{US}}$ . To properly measure the signal, lens 3 is added. It focuses the light on diode 1 to distinguish even closer peaks.

## 4 Execution of the Experiment

As described in [section 3](#), a HeNe-Laser is used to provide a collimated, continuous light beam for the experiment. Using two mirrors, the beam is directed onto the optical axis. First the Laser was turned on, after that the adjustment of the mirrors could begin. To get reliable results it is important that the light beam is centered on the optical axis and will not change in position or height until it reaches the diodes. This was ensured by placing a screen directly behind the beam splitter and moving it along the optical axis. Using the x-y-adjusting screws, both mirrors were tilted until the light beam was perfectly aligned on the optical axis.

The positions of the beam splitter and mirror 3 were not changed as their positioning is uncritical because the beam is already collimated. After that, lens 1 was placed on the optical axis. As its z-position is also uncritical, the lens was placed directly behind the beam splitter.

Taking the same x-y-adjustment steps, lens 2 was set onto the optical axis. As it is the purpose of those 2 lenses to widen the beam profile and recollimate the beam, the focal points of both lenses must lie exactly on top of each other. For the optimum distance we get  $l_1 = f_1 + f_2 = 150 \text{ mm}$ . This distance was first roughly adjusted using a ruler, then the collimation of the beam was tested. To do so, the rotating mirror was manually set to a position where the light beam is reflected in a direction close to the optical axis. This way, the beam profile could be examined over a length twice as long as the optical axis so that a good collimation could be reached by moving lens 2 until the diameter of the light beam stayed constant over this distance. The diameter was estimated, holding a piece of paper into the beam.

Next, the iris was placed directly behind lens 2. Again, it was checked that the position of the beam profile would not change. x- and y-adjustments were made accordingly. The diameter of the iris was chosen so that the edges of the beam profile were cleaned but the whole beam profile itself would pass. This was chosen because the beam would not be collimated any more if the iris was closed too far. Again the collimation was checked using the method described above. The beam diameter behind the iris  $d = (3.0 \pm 0.5)$  mm was measured a ruler and the scale paper on the screen. The uncertainty was estimated on basis of the blurry edges of the beam.

In part 1 of the experiment a sine amplitude grating is examined. The grating was placed directly behind the iris and the interference pattern was examined on scale paper on a screen. The screen was set to a position so that both first order maximum peaks were visible at the sides of the screen. The distance between the front side of the grating and the screen was estimated using a ruler which was held to the screen and aimed down at the grating so that the parallax error could be minimized.

In the next step, 5 amplitude gratings were examined after a calibration using the reference grating with known groove density. Therefore, the rotating mirror and both diodes were used. The position of the rotating mirror was not changed for this part. First, the trigger diode was positioned. Then, signal 2 was amplified and viewed on the oscilloscope and the height of the diode was adjusted until a clear signal was observable. After this, diode 1 was amplified and viewed on the oscilloscope using the signal coming from diode 2 as trigger. Diode 1 was again adjusted in height and position until a clear signal, similar to a gaussian pulse, was visible on the oscilloscope.

Unfortunately, the data measured with this setup did not match the expected interference patterns. Even the interference spectrum of the reference grating was hard to see and overlaid by a „underground“ peak which made it impossible to get reliable values for the peak positions and intensities. This was improved by swapping diodes 1 and 2. In addition to that, the gratings had to be rotated with respect to the optical axis so that possible distortions resulting from the rotating mirror could be compensated. The angle was measured using a triangle ruler, the uncertainty was estimated due to difficulties in estimating the course of the optical axis. A picture of the final setup is visible in [fig. 14](#).

For part 2 of the experiment, the gratings were removed and the ultrasound chamber was placed directly behind the iris. As the light beam is collimated, the positioning of the chamber is uncritical. Therefore, a positioning in which the the interference pattern caused by the diffraction in the ultrasonic chamber is generated far away from the diode could be chosen. This leads to a stronger widening to the interference pattern, and consequently to a better visibility of the pattern. To guarantee that the light beam is still positioned on the optical axis, the screen was again used to check its position. The chamber was slightly rotated to adjust it. To focus the interference pattern to diode 1, an additional lens was placed in front of the rotating mirror. The focal length equals  $f_3 = 300$  mm. Using a ruler, the distance between lens and diode was roughly estimated to match the focal length. Then, the rotating mirror was stopped again to reflect the light in a small angle to the optical axis. That way, the focus point of the lens could be found. The final positioning

was then performed using the output from the oscilloscope, adjusting the positions of lens and diode as well as the rotation angle of the diode until a clear peak could be observed. To do so, the position of the rotating mirror as well as the position of diode 2 had to be adjusted as well. After the positioning was finished, the ultrasound transmitter was turned on. The voltage amplitude was set to 10 V and the frequency to approximately 2000 kHz. Now, the frequency was modified over a range from 1800 kHz to 2350 kHz until a clear and mostly stable interference pattern was visible on the oscilloscope. This was the case for  $\nu = (2300.0 \pm 0.5)$  kHz. The uncertainty was estimated from the variations of the frequency during the measurement. After setting the frequency, the measurement could be carried out. For 21 different voltage amplitudes  $U_{\text{US}}$ , the interference pattern was viewed and saved with the oscilloscope. The uncertainty of the voltage amplitude was estimated to  $\sigma_{U_{\text{US}}} = 0.01$  V due to variations throughout the measurements. To find a conversion from the time differences on the oscilloscope to the corresponding angles, the reference grating was now placed in front of the ultrasonic chamber. This interference pattern at  $U_{\text{US}} = 0$  V was also saved. As in part 1 the grating had to be rotated by a certain angle to compensate distortions. A picture of this final setup is visible in [fig. 15](#).

## 5 Data Analysis

### 5.1 Grating Constant of a Sine Grating

The distance of the grating and the screen was determined to  $d = (12.9 \pm 0.2)$  cm. The wavelength of the laser  $\lambda = 632.8$  nm was taken from the instructions [1], it was assumed that the error on the wavelength is negligible. The scale paper on the screen was used to measure the position of the zeroth order maximum  $x_0 = (0.1 \pm 0.1)$  cm, the left first order maximum  $x_l = (-5.3 \pm 0.1)$  cm and the right first order maximum  $x_r = (5.6 \pm 0.1)$  cm. Next, the distance of the first order maxima to the zeroth maximum was determined by

$$r_r = x_r - x_0 \qquad r_l = x_0 - x_l.$$

The error is given by gaussian error propagation

$$s_{r_{r,l}} = \sqrt{2} \cdot s_x,$$

where  $s_x$  is the error on the position of the maxima. The mean of the distances to the right and the left maxima,

$$r = \frac{r_r + r_l}{2} \qquad s_r = \frac{1}{2} \sqrt{s_{r_r}^2 + s_{r_l}^2} = s_x,$$

was used for the distance  $r$  between the zeroth order maximum and the first order maxima needed for the calculation of the grating constant.

As only first order maxima were visible, the grating constant  $k_{\text{sin}}$  is given using [eq. \(2\)](#) with  $m = 1$  by

$$k = \frac{\lambda}{\sin \varphi}.$$

The sine of the angle  $\varphi$  in which the light of the first maxima hits the screen can be calculated using the distance  $d$  of grating to screen and the distance  $r$  of the first maxima to the zeroth maximum:

$$\sin \varphi = \frac{r}{\sqrt{d^2 + r^2}}.$$

The grating constant was calculated to

$$k_{\sin} = \lambda \frac{\sqrt{d^2 + r^2}}{r} = (1.63 \pm 0.04) \cdot 10^{-6} \text{ m}$$

The error is given by gaussian error propagation:

$$s_{k_{\sin}} = \sqrt{\left(\frac{\lambda d^2}{r^2 \sqrt{d^2 + r^2}} s_x\right)^2 + \left(\frac{\lambda d}{r \sqrt{d^2 + r^2}} s_d\right)^2},$$

## 5.2 Grating Constants of five Amplitude Gratings

### 5.2.1 Angle-Time Calibration

To be able to calculate the unknown grating constants of the amplitude gratings from the data measured with the oscilloscope later on, a reference grating with known grating constant was used to determine the angle-time conversion.

The groove density  $g_{\text{ref}} = 80$  lines per cm of the reference grating was taken from the instructions [1]. This was used to calculate the grating constant  $k_{\text{ref}} = 1/g_{\text{ref}} = 125 \mu\text{m}$ .

As the reference grating was rotated to the optical axis by an angle of  $\theta = (30 \pm 5)^\circ$ , the effective grating constant at which the diffraction occurs is given by

$$k_{\text{ref, eff}} = k_{\text{ref}} \cdot \cos \theta. \quad (12)$$

The uncertainty is given by

$$s_{k_{\text{ref, eff}}} = k_{\text{ref}} \cdot \sin \theta \cdot s_\theta. \quad (13)$$

The peaks of zeroth order were very high compared to the higher order maxima. Therefore, to determine the position and height of the maxima measured with best possible precision, both an overall dataset and a zoomed in dataset were used for each grating. As the intensity between the peaks did not reach zero, it was not sensible to try to determine the peak positions using a fit. Also, the theory predicts a sine-shape for the interference patterns (see eqs. (1) and (24)), and there is no theoretical foundation for the intensity pattern to follow a gaussian distribution. Therefore, it was not deemed sensible to use gaussian fits. Instead, the peak positions were determined by eye and the uncertainties were estimated taking the noise visible around the peaks into account.

The zoomed in interference pattern of the reference grating measured with the oscilloscope is pictured in fig. 2. The process for determining the peak positions was repeated for each of the gratings. The interference patterns with the peak positions are depicted in figs. 16 to 21 in appendix A.1.

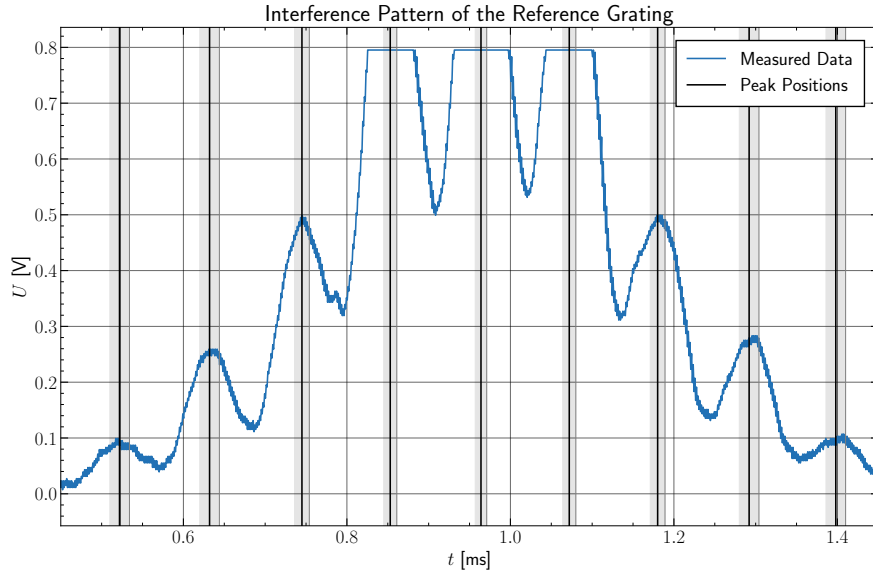


**Figure 2:** Interference pattern of the reference grating measured using the oscilloscope, zoomed in to make the higher order maxima visible. The peak positions and their uncertainty were determined by eye.

To calculate the displacement  $t_{m,\text{rel}}$  of the higher order maxima to the zeroth order maximum, the difference

$$t_{m,\text{rel}} = t_m - t_0 \quad s_{t_{m,\text{rel}}} = \sqrt{s_{t_m}^2 + s_{t_0}^2} . \quad (14)$$

where  $t_i$  is the peak position of the  $i$ -th maximum, was taken. The uncertainty is given by gaussian error propagation.

As the grating constant of the reference grating is known, the angles corresponding to the peak positions can be calculated by

$$\varphi_m = \frac{m \cdot \lambda}{k_{\text{ref, eff}}} \quad s_{\varphi_m} = \frac{m \cdot \lambda}{k_{\text{ref, eff}}^2} s_{k_{\text{ref, eff}}} , \quad (15)$$

using eq. (2) in a small-angle approximation. The calculated angles  $\varphi_m$  were plotted against the corresponding time measured with the oscilloscope. The resulting graph can be seen in fig. 3.

A weighted linear fit of the form  $\varphi(t) = \alpha t + \beta$  was performed using `scipy.odr`, which takes both  $x$  and  $y$  uncertainties into account.

The fit is also visible in fig. 3. The optimal values for the parameters are given by

$$\begin{aligned} \alpha &= (3.06 \pm 0.08)^\circ \text{ms}^{-1} \\ \beta &= (0.006 \pm 0.018)^\circ . \end{aligned} \quad (16)$$

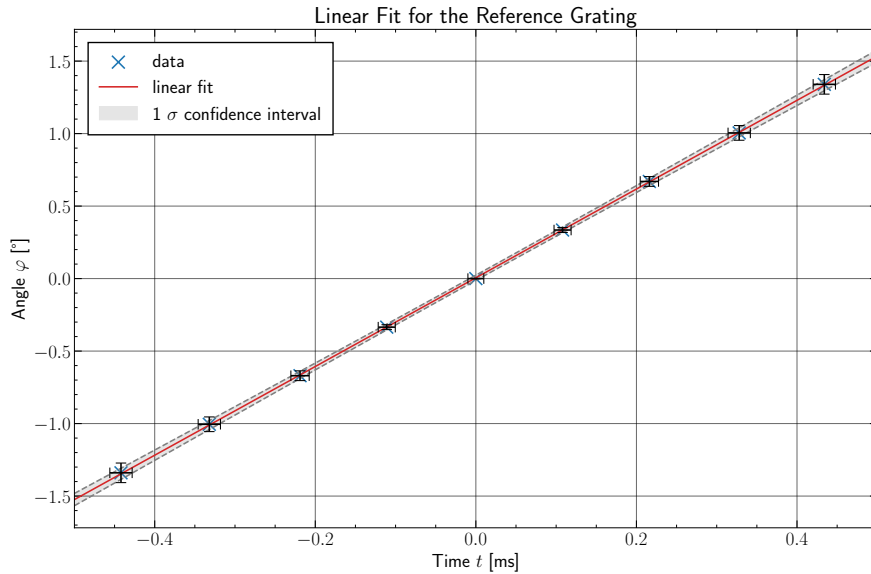


**Figure 3:** Angles  $\varphi$  of interference maxima of the reference grating plotted against the corresponding times  $t$  measured by the oscilloscope. A weighted linear fit of the form  $\varphi(t) = \alpha t + \beta$  was performed using `scipy.odr`. The optimal parameters can be found in eq. (16). A  $1\sigma$  confidence interval was also calculated.

### 5.2.2 Grating Constants of the five Amplitude Gratings

The peak positions of the interference maxima of the unknown gratings were determined analogously to the reference grating. The peak positions can be seen in figs. 16 to 21 in appendix A.1.

The time displacement of the peaks was calculated using eq. (14).

Using

$$\varphi(t) = \alpha t + \beta \quad (17)$$

with the parameters in eq. (16) resulting from the calibration, the angles corresponding to the peak positions can be calculated. The uncertainties of the angles are calculated with gaussian error propagation and are given by

$$s_\varphi = \sqrt{(s_\alpha \cdot t_{\text{rel}})^2 + (\alpha \cdot s_{t_{\text{rel}}})^2 + (s_\beta)^2}, \quad (18)$$

where again  $t_{\text{rel}}$  describes the relative times of the peaks to the zeroth order peak.

Using eqs. (12) and (15), the grating constants  $k$  of the unknown gratings can be calculated by

$$k = \frac{m \cdot \lambda}{\varphi \cdot \cos \theta} \quad (19)$$

with an uncertainty of

$$s_k = \sqrt{\left(\frac{m \cdot \lambda}{\varphi^2 \cdot \cos \theta} s_\varphi\right)^2 + \left(\frac{m \cdot \lambda \cdot \sin \theta}{\varphi \cdot \cos^2 \theta} s_\theta\right)^2}. \quad (20)$$

This was done for each peak. Finally, the mean of all  $k$  values was taken to get a single result for each grating. The resulting grating constants are listed in [table 1](#).

### 5.2.3 Resolution of five Amplitude Gratings

The resolution can be calculated from [eqs. \(6\) and \(7\)](#) using the beam width  $d = (3.0 \pm 0.5)$  mm and the highest visible order  $m_{\max}$  by

$$a = m_{\max} \cdot \frac{d}{k} \quad s_a = \sqrt{\left(\frac{m_{\max}}{k} s_d\right)^2 + \left(\frac{m_{\max} \cdot d}{k^2} s_k\right)^2} \quad (21)$$

The highest visible order was read from the interference patterns ([figs. 16 to 21](#) in [appendix A.1](#)). The calculated resolutions are listed in [table 1](#).

Grating	Grating Constant [ $\mu\text{m}$ ]	Highest Order	Resolution
1	$97 \pm 7$	4	$120 \pm 20$
2	$35 \pm 2$	2	$340 \pm 60$
3	$100 \pm 9$	3	$120 \pm 20$
4	$84 \pm 8$	3	$140 \pm 30$
5	$53 \pm 3$	3	$230 \pm 40$

**Table 1:** Calculated grating constants and resolutions for each of the five unknown gratings. The highest visible order of each grating is also listed.

### 5.2.4 Aperture Function of Grating 1

The heights and corresponding uncertainties of the peaks in the interference pattern of grating 1 were determined by eye. They are visible in [fig. 4](#), the values are listed in [table 2](#).

Order	t [ $\mu\text{s}$ ]	U [V]
-4	$512 \pm 20$	$0.12 \pm 0.08$
-3	$597 \pm 15$	$0.29 \pm 0.08$
-2	$682 \pm 10$	$0.49 \pm 0.04$
-1	$778 \pm 10$	$0.74 \pm 0.04$
0	$946 \pm 7$	$6.40 \pm 0.08$
1	$1122 \pm 12$	$0.73 \pm 0.05$
2	$1216 \pm 12$	$0.47 \pm 0.04$
3	$1307 \pm 12$	$0.26 \pm 0.04$
4	$1400 \pm 15$	$0.13 \pm 0.06$

**Table 2:** Estimated peak positions of the interference maxima of grating 1 as well as their height.

As there are two voltages  $U^{m,l}$  and  $U^{m,r}$  for each order  $m$ , the mean

$$U^m = \frac{U^{m,l} + U^{m,r}}{2} \quad s_{U^m} = \frac{1}{2} \sqrt{s_{U^{m,l}}^2 + s_{U^{m,r}}^2} \quad (22)$$

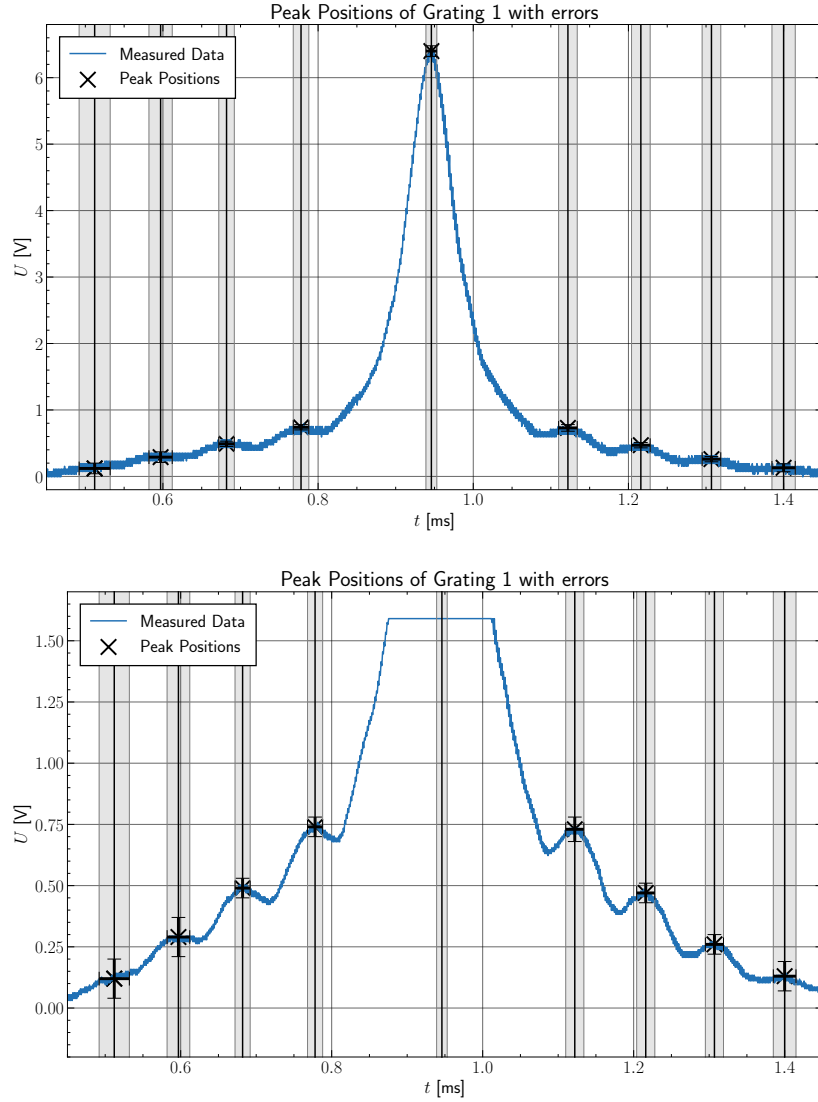


**Figure 4:** Interference pattern of grating 1 measured by the oscilloscope. The peak positions and amplitudes were determined by eye.

was taken to determine a voltage  $U^m$  for each order.

To calculate the aperture function, the voltages  $U^m$  have to be scaled with respect to  $U^0$ :

$$U_m = \frac{U^m}{U^0}. \quad (23)$$

The scaled voltages can then be used to approximate the aperture function with eq. (3). The resulting function is

$$g(x) = \sum_{j=0}^4 \sqrt{U_j} \cdot \cos 2\pi j \frac{x}{k_1}, \quad (24)$$

where  $k_1$  is the calculated grating constant of grating 1 listed in table 1.

The aperture function of grating 1 is depicted in [fig. 5](#).

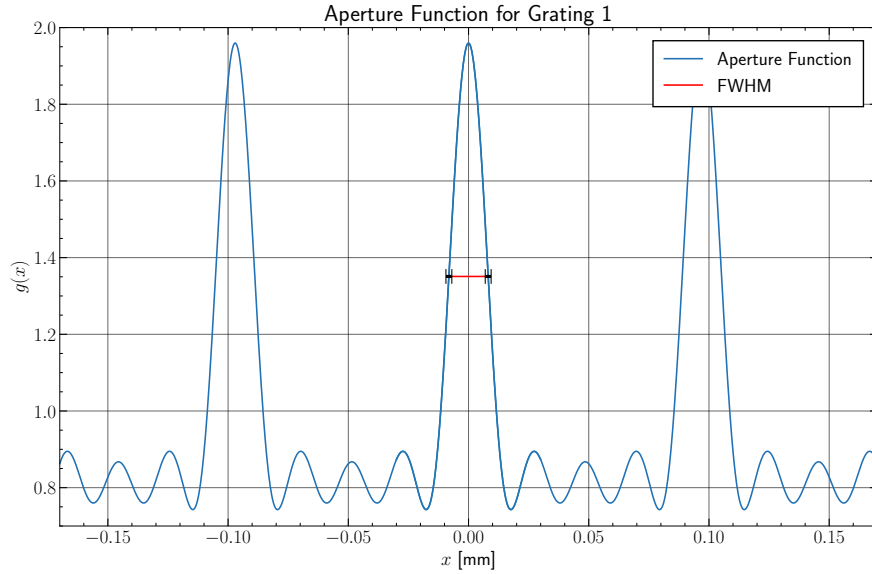


**Figure 5:** Aperture function  $g(x)$  of grating 1 calculated in [eq. \(24\)](#). The FWHM was calculated using `scipy.interpolate.UnivariateSpline`, the uncertainties were estimated.

### 5.2.5 Proportion of Slit Width and Grating Constant of Grating 1

As the unapproximated aperture function for an amplitude grating is a rectangle function, the full width at half maximum (FWHM) of the aperture function was used for the slit width  $b$ . The FWHM

$$b = (16.3 \pm 1.7) \mu\text{m}$$

was calculated using `scipy.interpolate.UnivariateSpline`, the uncertainty estimated based on the preceding uncertainties. The aperture function as well as the FWHM are depicted in [fig. 5](#).

The proportion  $p$  of the slit width to the grating constant  $k_1$  of grating 1 is given by

$$p = \frac{b}{k_1} = 0.168 \pm 0.021,$$

the uncertainty

$$s_p = \sqrt{\left(\frac{b \cdot s_{k_1}}{k_1^2}\right)^2 + \left(\frac{1}{k_1} \cdot s_b\right)^2}$$

was calculated with gaussian error propagation.

## 5.3 Examination of the Phase Grating

As described in [section 4](#), the frequency of the ultrasonic chamber was set to

$$\nu = (2300.0 \pm 0.5) \text{ kHz.}$$

For 21 different voltage amplitudes of the quartz crystals, from  $(0.00 \pm 0.01)$  V to  $(10.24 \pm 0.01)$  V, the interference patterns were taken examined.

## 5.4 Comparison to the Raman-Nath-Theory

Plotting the different interference patterns against the corresponding voltage amplitudes leads to a 3-dimensional plot, visible in [fig. 6](#).

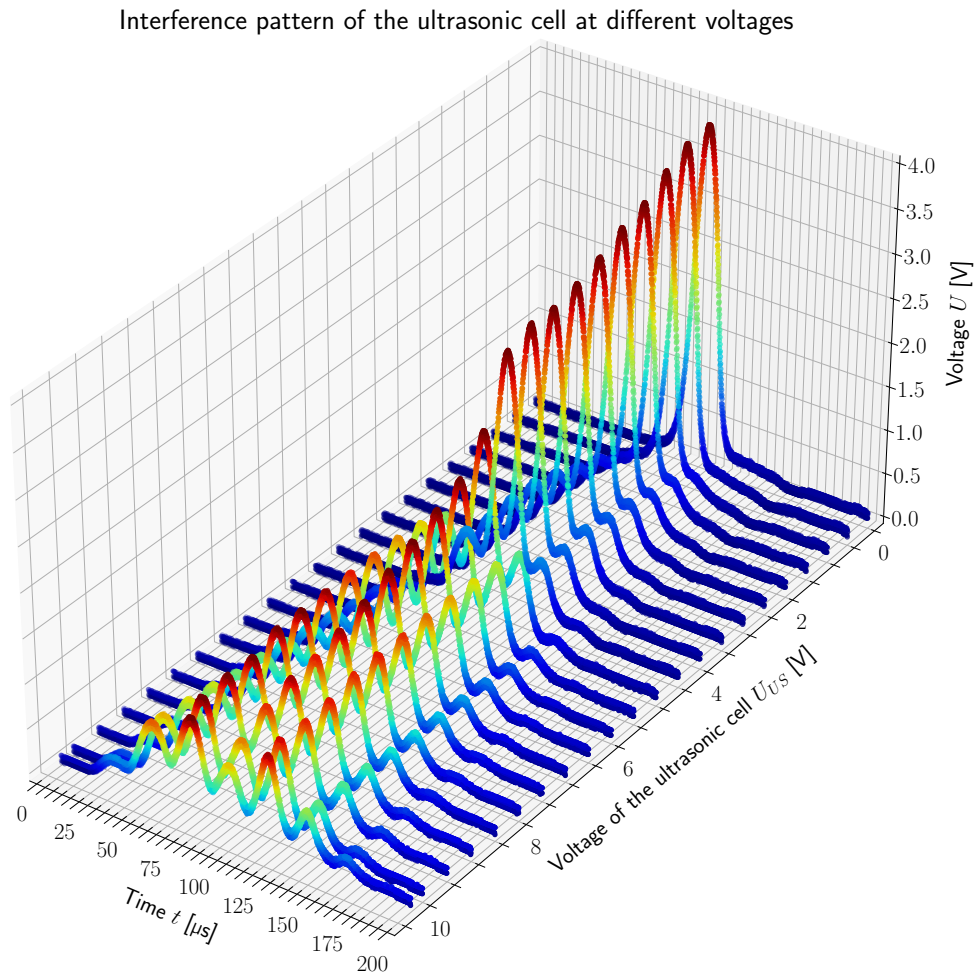


**Figure 6:** Interference pattern of the ultrasonic chamber at  $\nu = (2300.0 \pm 0.5)$  kHz with different voltage amplitudes from  $(0.00 \pm 0.01)$  V to  $(10.24 \pm 0.01)$  V. To acquire the data, the setup depicted in [fig. 1](#) was used and slightly modified by removing grating in front of the ultrasonic chamber.

As predicted by the Raman-Nath-Theory, the widening of the light beam and the shifting of the intensities can be seen. As the voltage of the ultrasonic chamber is increased, the 0-order maximum decreases in height while the higher order maxima arise.

To quantify this effect the amplitudes of each peak have been graphically estimated. The height uncertainties were set to comparably high values due to amplitude fluctuations throughout the measurement. The interference-patterns with the estimated peak-positions and intensities can be seen in [figs. 22 to 32](#) in [appendix A.1](#). According to the Raman-Nath-Theory, described in [section 2](#), the peak intensities of the  $m$ -order maximum peaks at different voltages can be described using the Bessel-J-function ([eq. \(11\)](#)). To verify this theory, the peak intensities  $I$  were plotted against the corresponding voltage amplitudes  $U_{\text{US}}$  at the quartz-crystals for the different orders  $m$  in the interference pattern. For this, the average of the heights of the positive and negative order maximum peaks was taken, scaled and the uncertainties were computed using gaussian error propagation. The values have to be scaled so that the 0-order maximum peak at  $U_{\text{US}} = 0 \text{ V}$  occurs at intensity 1 to fit the Bessel-functions height.

$$I = \frac{1}{h_{0,0\text{V}}} \frac{h_{+m} + h_{-m}}{2} \quad (25)$$

$$s_I = \sqrt{\left( \frac{1}{h_{0,0\text{V}}^2} \frac{h_{+m} + h_{-m}}{2} \cdot s_{h_{0,0\text{V}}} \right)^2 + \left( \frac{h_{+m}}{2 \cdot h_{0,0\text{V}}} \cdot s_{h_{-m}} \right)^2 + \left( \frac{h_{-m}}{2 \cdot h_{0,0\text{V}}} \cdot s_{h_{+m}} \right)^2}$$

To find the fit-parameter  $\alpha$  from [eq. \(11\)](#), the Bessel-fits were performed using `scipy.optimize.curve_fit` with the Bessel-J-function `scipy.special.jv`. The resulting intensities and fits for the orders  $m = [0, 1, 2, 3]$  can be found in [figs. 7 to 10](#).

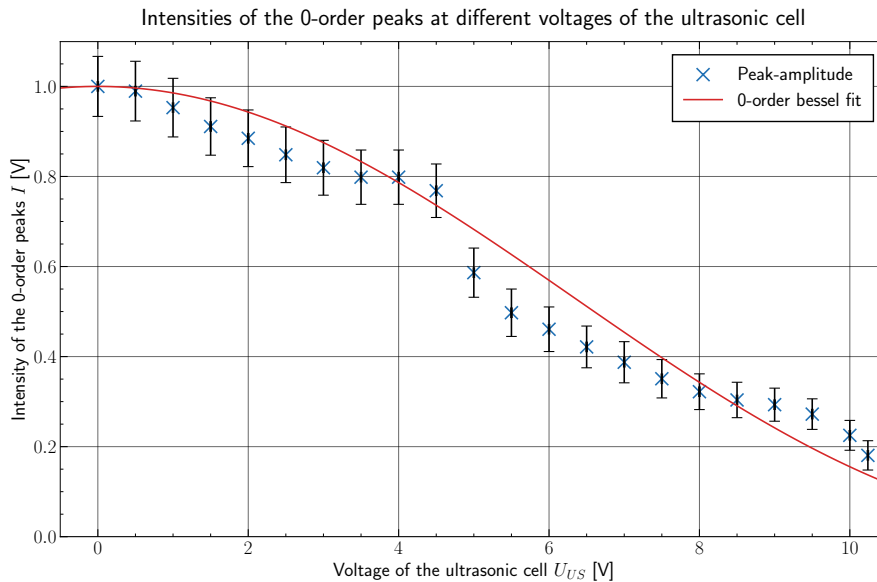


**Figure 7:** Intensities of the 0-order maximum peaks, using the the ultrasonic chamber as a phase-grid at different voltages  $U_{\text{US}}$ . The peak heights and uncertainties were estimated and converted to intensities using [eq. \(25\)](#). The Bessel-fits were performed using `scipy.optimize.curve_fit` and `scipy.special.jv`, according to the Raman-Nath-Theory in [eq. \(11\)](#). The raw outputs from the oscilloscope can be found in [figs. 22 to 32](#).

The optimal fit parameter  $\alpha$  and the reduced  $\chi^2_{\nu}$ -value for each fit can be found in [table 3](#).

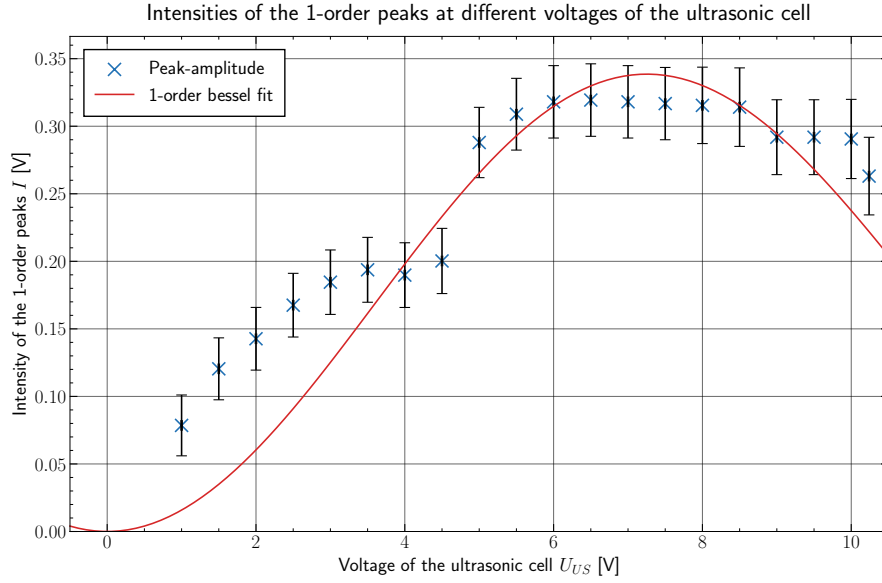


**Figure 8:** Intensities of the 1-order maximum peaks, using the the ultrasonic chamber as a phase-grid at different voltages  $U_{US}$ . The peak heights and uncertainties were estimated and converted to intensities using eq. (25). The Bessel-fits were performed using `scipy.optimize.curve_fit` and `scipy.special.jv`, according to the Raman-Nath-Theory in eq. (11). The raw outputs from the oscilloscope can be found in figs. 22 to 32.

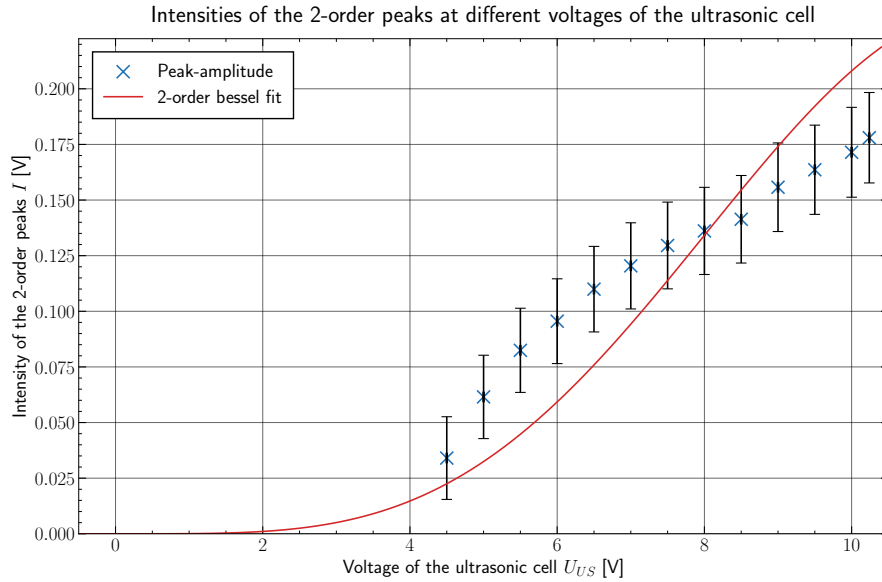


**Figure 9:** Intensities of the 2-order maximum peaks, using the the ultrasonic chamber as a phase-grid at different voltages  $U_{US}$ . The peak heights and uncertainties were estimated and converted to intensities using eq. (25). The Bessel-fits were performed using `scipy.optimize.curve_fit` and `scipy.special.jv`, according to the Raman-Nath-Theory in eq. (11). The raw outputs from the oscilloscope can be found in figs. 22 to 32.

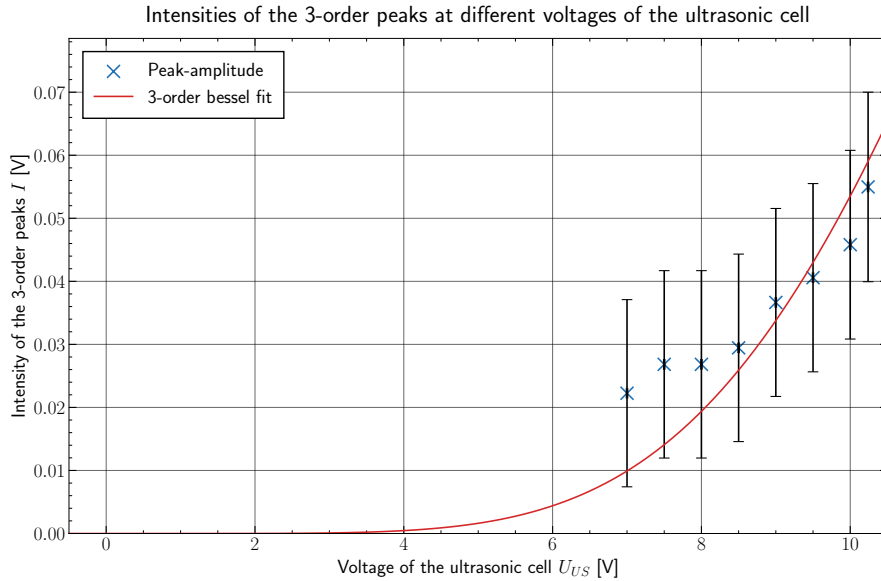


**Figure 10:** Intensities of the 3-order maximum peaks, using the ultrasonic chamber as a phase-grid at different voltages  $U_{US}$ . The peak heights and uncertainties were estimated and converted to intensities using eq. (25). The Bessel-fits were performed using `scipy.optimize.curve_fit` and `scipy.special.jv`, according to the Raman-Nath-Theory in eq. (11). The raw outputs from the oscilloscope can be found in figs. 22 to 32.

$m$	$\alpha$ [ $V^{-1}$ ]	$\chi^2_{\nu}$
0	$0.171 \pm 0.002$	1.86
1	$0.254 \pm 0.005$	3.34
2	$0.258 \pm 0.005$	2.16
3	$0.258 \pm 0.009$	0.305

**Table 3:** Optimal parameters  $\alpha$  for the Bessel-fits using the Raman-Nath-Theory from eq. (11) and corresponding reduced  $\chi^2$ -values for the different visible orders  $m$ . The Bessel-fits were performed using `scipy.optimize.curve_fit` and `scipy.special.jv`, according to the Raman-Nath-Theory in eq. (11). The raw outputs from the oscilloscope can be found in figs. 22 to 32.

## 5.5 Calculation of the wavelength in isoctane

In the next step, the interference pattern itself is examined. As described above, the peak-positions have been estimated for the pattern at a voltage of  $U_{US} = (10.24 \pm 0.01)$  V. These can be seen in fig. 11 and table 5.

As before, a calibration using the reference grating is necessary to interpret the data. The reference grating placed in front of the ultrasonic chamber had to be rotated by an angle of  $\theta = (17 \pm 2)^\circ$  to get a clear, symmetrical interference pattern, visible in fig. 12. The values for the peak positions can be found in table 4.

Following the steps as described in section 5.2.1, the angle-time-calibration was performed

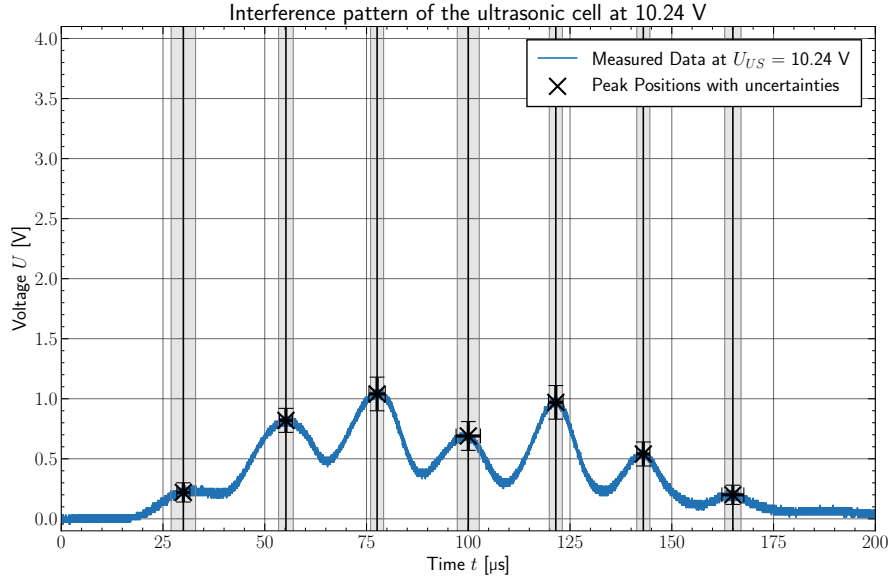


**Figure 11:** Interference pattern of the ultrasonic chamber at  $\nu = (2300.0 \pm 0.5)$  kHz with a voltage amplitude of  $U_{US} = (10.24 \pm 0.01)$  V. To acquire the data, the setup depicted in [fig. 1](#) was used, without the grating in front of the ultrasonic chamber. The positions and uncertainties of the peaks were estimated and can be found in [table 5](#).

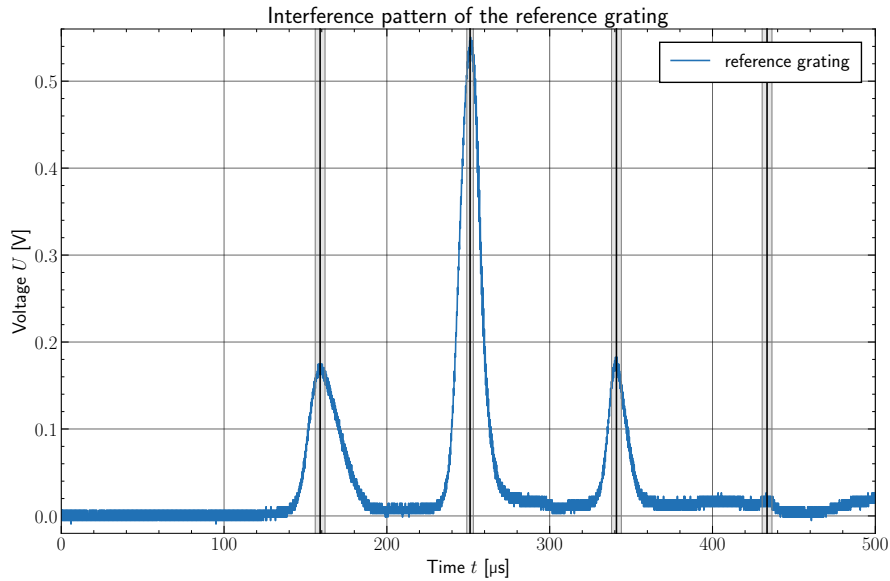


**Figure 12:** Interference pattern of the calibration grating with a groove density of  $g_{\text{ref}} = 80$  L/cm placed in front of the ultrasonic chamber with a voltage amplitude of  $U_{US} = 0$  V. To acquire the data, the setup depicted in [fig. 1](#) was used. The positions and uncertainties of the peaks were estimated and can be found in [table 4](#).

using a weighted linear regression considering the x- and y-uncertainties with `scipy.odr`. The result can be seen in [fig. 13](#), the optimal fit parameters for the linear fit with  $\varphi(t) = at + \beta$  in [eq. \(26\)](#).

$m$	$t$ [ $\mu\text{s}$ ]	$t_{\text{rel}}$ [ $\mu\text{s}$ ]
-1	$159 \pm 3$	$-92 \pm 4$
0	$251 \pm 2$	$0 \pm 3$
1	$341 \pm 3$	$90 \pm 4$
2	$433 \pm 3$	$182 \pm 4$

**Table 4:** Peak positions of the different order maxima from the reference grating. The ultrasonic chamber was still positioned on the optical axis, but not turned on. The values and uncertainties have been estimated, taking the visible fluctuations throughout the experiment into account. As the groove density is known, a calibration from angle to time can be made.

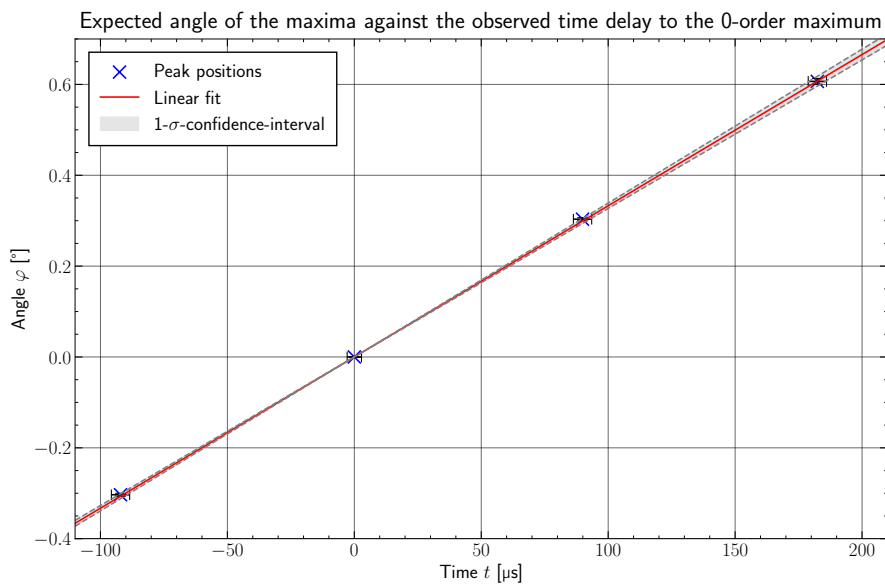


**Figure 13:** Angles  $\varphi$  of interference maxima of the reference grating plotted against the corresponding times  $t$  measured by the oscilloscope. A weighted linear fit of the form  $\varphi(t) = \alpha t + \beta$  was performed using `scipy.odr`. The optimal parameters can be found in eq. (16). A 1- $\sigma$ -confidence-interval was also calculated.

$$\begin{aligned}\alpha &= (3.33 \pm 0.06)^\circ \text{ms}^{-1} \\ \beta &= (0 \pm 5) \cdot 10^{-19}^\circ\end{aligned}\tag{26}$$

Using this correlation, the angles can be calculated for the peaks visible in the interference spectrum with the ultrasonic chamber. The uncertainties were calculated using gaussian error propagation, as described in section 5.2.1.

Using eq. (10), the grating constant of the ultrasonic chamber at the provided frequency can be calculated with

$$\Lambda_{\text{meas.}} = \frac{m\lambda}{\varphi} \qquad s_{\Lambda_{\text{meas.}}} = \left| \frac{m\lambda}{\varphi^2} \cdot s_{\varphi} \right|\tag{27}$$

$m$	$t$ [ $\mu\text{s}$ ]	$t_{\text{rel}}$ [ $\mu\text{s}$ ]	$\varphi$ [ $^\circ$ ]
-3	$30 \pm 3$	$-70 \pm 4$	$-0.233 \pm 0.014$
-2	$55.2 \pm 1.8$	$-45 \pm 3$	$-0.149 \pm 0.011$
-1	$77.6 \pm 1.6$	$-22 \pm 3$	$-0.075 \pm 0.011$
0	$100 \pm 3$	$0 \pm 4$	$0.000 \pm 0.013$
1	$121.5 \pm 1.6$	$22 \pm 3$	$0.072 \pm 0.011$
2	$143.0 \pm 1.6$	$43 \pm 3$	$0.143 \pm 0.011$
3	$165 \pm 2$	$65 \pm 3$	$0.216 \pm 0.012$

**Table 5:** Peak positions, relative peak positions and angles of the different order maxima of the ultrasonic chamber at  $\nu = (2300.0 \pm 0.5)$  kHz and  $U_{\text{US}} = (10.24 \pm 0.01)$  V. The values and uncertainties have been estimated considering the visible fluctuations throughout the experiment. The angles have been calculated using the linear regression from [fig. 13](#) and [eq. \(26\)](#).

using the small-angle approximation for  $\varphi \ll 1$ . For each Peak in [fig. 11](#),  $\Lambda$  was calculated and the average was taken. Again, gaussian error propagation was used for the corresponding uncertainty. The theoretically predicted value for the wave length can be calculated using the applied frequency and the speed of sound in isooctane  $c_{\text{iso}} = 1111$  m/s [2]. The wave length can then be calculated using

$$\Lambda_{\text{lit.}} = \frac{c_{\text{iso}}}{\nu} \qquad s_{\Lambda_{\text{lit.}}} = \frac{c_{\text{iso}}}{\nu^2} s_{\nu}. \qquad (28)$$

Using the value for the frequency and the calculated angles, one gets

$$\begin{aligned} \Lambda_{\text{meas.}} &= (490 \pm 20) \mu\text{m} \\ \Lambda_{\text{theo.}} &= (483.04 \pm 0.11) \mu\text{m}. \end{aligned}$$

## 6 Summary and Discussion

### 6.1 Sine Grating

The grating constant of the sine grating was calculated to

$$k_{\text{sin}} = (1.62 \pm 0.04) \mu\text{m}.$$

The measurements were precise enough to determine the grating constant to a relative uncertainty of 2.6 %.

As the literature value for the grating constant is unknown, it is not possible to compare the calculated value to it. While the calculated grating constant for the sine grating is significantly smaller than the constants for the other amplitude gratings, it still seems to be a reasonable value.

### 6.2 Amplitude Gratings

Using the reference grating, an angle-time calibration was possible which was then used to calculate the grating constants and resolution of the five unknown gratings. The grating constants, resolution as well as their relative errors are listed in [table 6](#).

Grating	$k$ [ $\mu\text{m}$ ]	$s_k/k$ [%]	Resolution $a$	$s_a / a$ [%]
1	$97 \pm 7$	6.8	$120 \pm 20$	18
2	$35 \pm 2$	5.6	$340 \pm 60$	18
3	$100 \pm 9$	9.4	$120 \pm 20$	19
4	$84 \pm 8$	9.0	$140 \pm 30$	19
5	$53 \pm 3$	6.0	$230 \pm 40$	17

**Table 6:** Calculated grating constants  $k$  and resolutions  $a$  for each of the five unknown gratings. The relative errors  $s_k/k$  and  $s_a/a$  on the calculated values are also listed.

As with the sine grating, reference values for the grating constants were not given, so it is not possible to verify the results. However, given that the relative errors are all under 10 %, it can be said that it was possible to determine the grating constants to a satisfactory precision. The relative error for the resolutions on the other hand is rather large. To determine the resolution more precisely, it is necessary to get a better measurement of the beam width as well as the grating constants.

For grating 1, the amplitude of the peaks were determined. They are shown in [fig. 4](#), the values are listed in [table 2](#). This was used to approximate the aperture function, which is depicted in [fig. 5](#). The aperture function has the expected shape and can reasonably be assumed to approximate a rectangle function for a large number of observed maxima. The maxima of the aperture function, which should be 1 for 100 % transmission in a rectangle function, seem to be around 2. However, with a larger number of observed maxima it is quite possible for the maximum height to lower to about 1.

Using the FWHM of the aperture function and the grating constant, the proportion of the slit width to the grating constant

$$p = 0.168 \pm 0.021$$

was calculated.

As no reference value was given, it is not possible to verify this result. The magnitude seems reasonable, and with a relative uncertainty of 6.8% it was possible to reach a satisfactory precision. However, as with the aperture function, the validity of this result is restricted by the approximation made in calculating the aperture function.

### 6.3 Phase Gratings

The amplitudes of the visible peaks were used to verify the Raman-Nath-Theory. For each maximum order a Bessel-fit was performed accordingly as visible in [figs. 7 to 10](#). The optimal parameters as well as their fit uncertainties, relative uncertainties and reduced  $\chi^2$ -values are listed in [table 7](#).

$m$	$\alpha$ [ $V^{-1}$ ]	$s_\alpha/\alpha$ [%]	$\chi^2_\nu$
0	$0.171 \pm 0.002$	1.5	1.86
1	$0.254 \pm 0.005$	1.9	3.34
2	$0.258 \pm 0.005$	2.1	2.16
3	$0.258 \pm 0.009$	3.4	0.305

**Table 7:** Optimal fit parameters for the Bessel-fits stated in [eq. \(11\)](#), relative uncertainties and corresponding reduced  $\chi^2$ -values for the different orders  $m$ .

As the relative uncertainties, which are under 5%, are quite low, no strong deviation from the theory can be observed. However, the reduced  $\chi^2$ -values are comparably high resulting from the well visible fluctuations of the data around the model functions in [figs. 7 to 10](#). This could already be expected during the experiment as the amplitudes of the peaks were unstable in their intensity. Also, sudden changes in the intensities were visible on the oscilloscope while the measurement was taken, explaining for example the visible leaps in [figs. 7 and 8](#).

Using the peak positions of the maxima, the wave length of the ultrasonic wave in the isoctane could be estimated to

$$\Lambda_{\text{meas.}} = (490 \pm 20) \mu\text{m} \qquad \frac{s_{\Lambda_{\text{meas.}}}}{\Lambda_{\text{meas.}}} = 4.1 \%$$

after an angle-time calibration using the reference grating.

Considering the speed of sound in isoctane and the provided frequency, a comparative value could be calculated to

$$\Lambda_{\text{theo.}} = (483.04 \pm 0.11) \mu\text{m} \qquad \frac{s_{\Lambda_{\text{meas.}}}}{\Lambda_{\text{meas.}}} = 0.023 \%$$

If we consider the values and uncertainties contributing to both wave lengths, the relative uncertainties seem reasonable and satisfactory. Comparing both values leads to a  $t$ -value of  $t = 0.35$ . This highly indicates a good accordance between the Raman-Nath-Theory and the actual wave length.

All in all, it can be said that the Raman-Nath-Theory is in good accordance with the measurements. For this reason, performing the given measurements, the validity of the Raman-Nath-Theory can be presumed.

## A Appendix

### List of Figures

1	Schematic structure of the used setup . . . . .	5
2	Grating 1 Peak Positions zoomed in . . . . .	10
3	Time-Angle Calibration Fit . . . . .	11
4	Grating 1 Peak Positions with Height . . . . .	13
5	Grating 1 Aperture Function . . . . .	14
6	Interference pattern of the ultrasonic chamber at different voltages $U_{US}$ . .	15
7	Intensities of the 0-order maximum peaks at different voltages $U_{US}$ . . . . .	16
8	Intensities of the 1-order maximum peaks at different voltages $U_{US}$ . . . . .	17
9	Intensities of the 2-order maximum peaks at different voltages $U_{US}$ . . . . .	17
10	Intensities of the 3-order maximum peaks at different voltages $U_{US}$ . . . . .	18
11	Interference pattern of the ultrasonic chamber at maximum voltage intensity	19
12	Interference pattern of the calibration grating with ultrasonic chamber . .	19
13	Angle-Time-Calibration for the setup with the ultrasonic chamber . . . . .	20
14	Picture of the setup for the measurement in part 1 . . . . .	27
15	Picture of the setup for the measurement in part 2 . . . . .	27
16	Reference Grating Peak Positions . . . . .	28
17	Peak Positions of Grating 1 . . . . .	28
18	Peak Positions of Grating 2 . . . . .	28
19	Peak Positions of Grating 3 . . . . .	29
20	Peak Positions of Grating 4 . . . . .	29
21	Peak Positions of Grating 5 . . . . .	29
22	Ultrasonic Chamber 0 V Peak Positions . . . . .	30
23	Ultrasonic Chamber 1 V Peak Positions . . . . .	30
24	Ultrasonic Chamber 2 V Peak Positions . . . . .	30
25	Ultrasonic Chamber 3 V Peak Positions . . . . .	31
26	Ultrasonic Chamber 4 V Peak Positions . . . . .	31
27	Ultrasonic Chamber 5 V Peak Positions . . . . .	31
28	Ultrasonic Chamber 6 V Peak Positions . . . . .	32
29	Ultrasonic Chamber 7 V Peak Positions . . . . .	32
30	Ultrasonic Chamber 8 V Peak Positions . . . . .	32
31	Ultrasonic Chamber 9 V Peak Positions . . . . .	33
32	Ultrasonic Chamber 10 V Peak Positions . . . . .	33

## List of Tables

1	Grating constants and resolutions for the five amplitude gratings . . . . .	12
2	Peak positions and heights of grating 1 . . . . .	12
3	Parameters and reduces $\chi^2_\nu$ values for the Bessel-fits . . . . .	18
4	Peak positions of the reference grating with the ultrasonic chamber turned off	20
5	Peak positions with the ultrasonic chamber at $U_{\text{US}} = (10.24 \pm 0.01) \text{ V}$ . . .	21
6	Grating constants, resolutions and relative uncertainties for the five amplitude gratings . . . . .	22
7	Parameters, relative uncertainties and $\chi^2_\nu$ -values for the Bessel-fits . . . . .	23

## Bibliography

- [1] M. Köhli, *Fortgeschrittenen Praktikum Teil I, Ultraschall* (Institute of Physics, University of Freiburg, 2011, Sept. 7, 2022).
- [2] Lutz Lefèvre, *Beugung am Amplitudengitter und Phasengitter, Versuchsaufbau für das Fortgeschrittenen-Praktikum* (Institute of Physics, University of Freiburg, 1977, Sept. 7, 2022).
- [3] D. T. Pierce and R. L. Byer, *Experiments on the Interaction of Light and Sound for the Advanced Laboratory* (Applied Physics Department, Stanford University, 1972, Sept. 7, 2022).
- [4] C. V. Raman and N. S. Nagendra Nath, *The Diffraction of Light by High Frequency Sound Waves: Part I* (Department of Physics, Indian Institute of Science, Bangalore, 1935, Sept. 7, 2022).

## Final setup for part 1

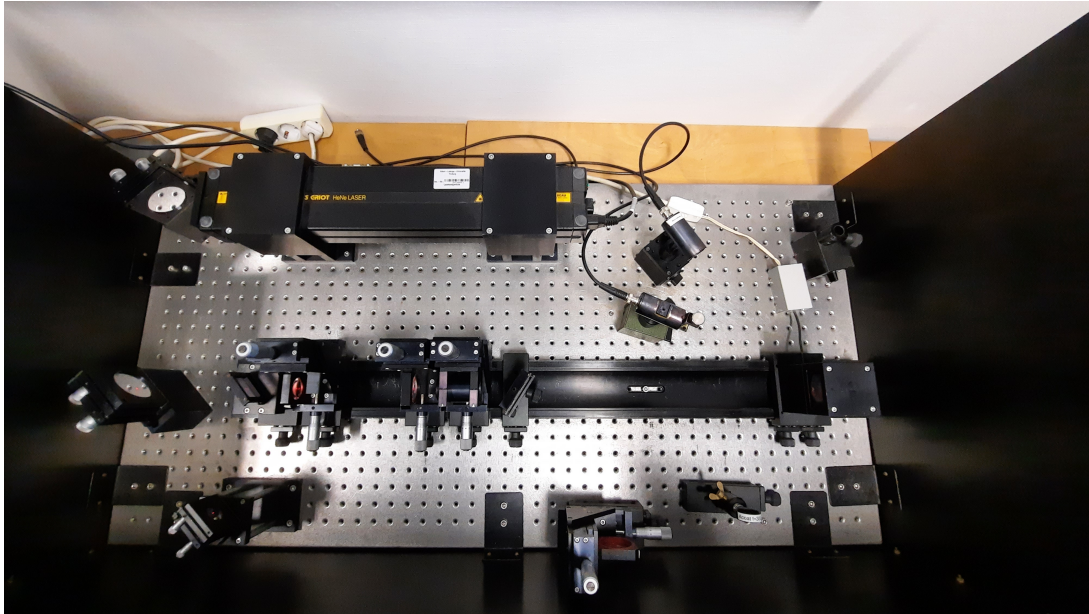


**Figure 14:** Picture of the final setup for the measurement in part 1. As it can be seen, the grating placed at the center of the optical axis had to be rotated to compensate distortions from the rotating mirror.

## Final setup for part 2

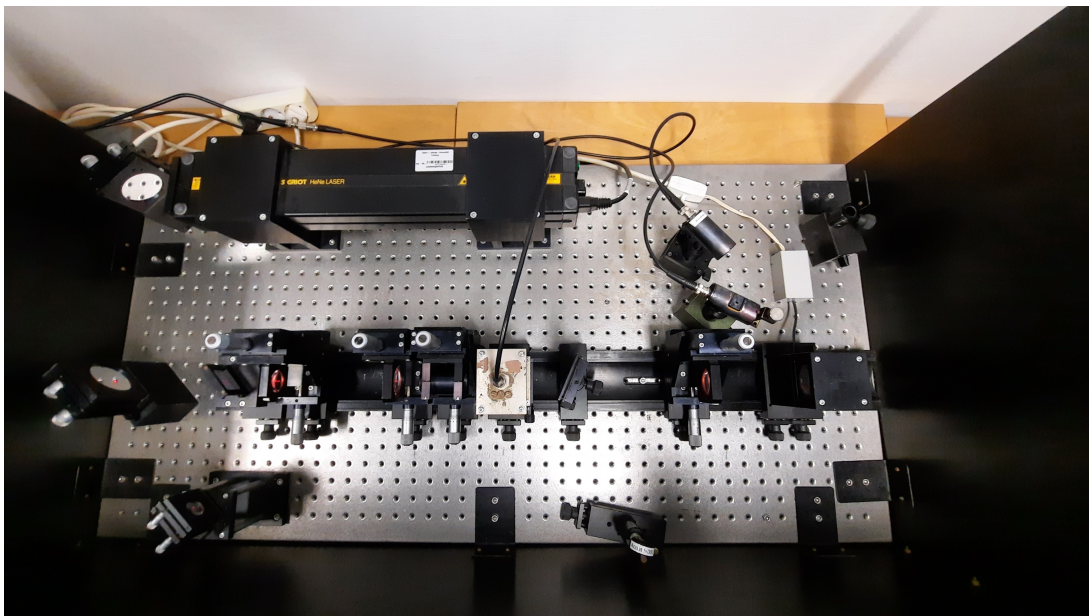


**Figure 15:** Picture of the final setup for the measurement in part 2. As it can be seen, the grating placed at the center of the optical axis had to be rotated to compensate distortions from the rotating mirror. The distance between lens 3 and diode 1 matches the focal length so that the diode can record a focused interference pattern.

### A.1 Interference Pattern for each Grating

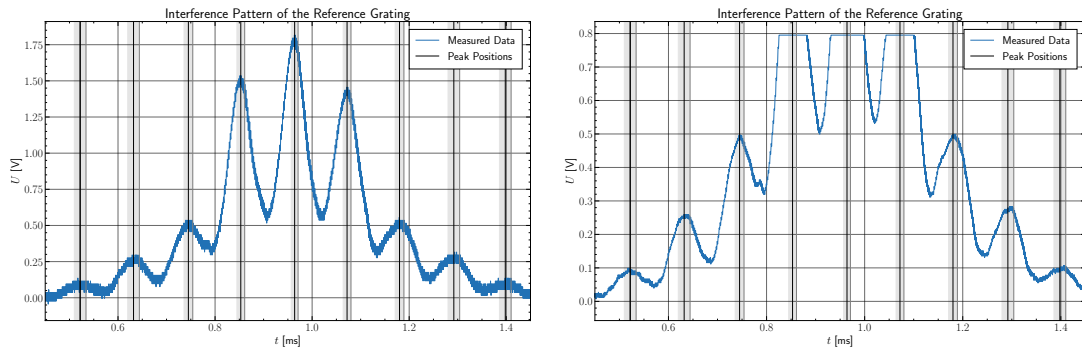


**Figure 16:** Interference Pattern for the reference grating and the determined peaks.

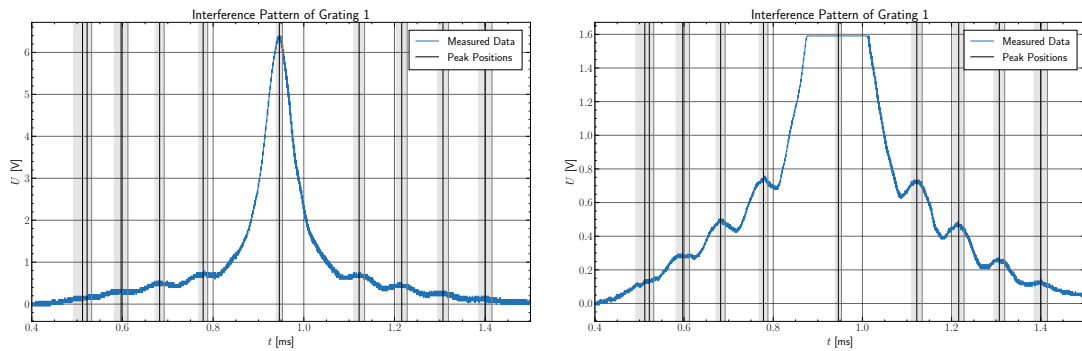


**Figure 17:** Interference Pattern for grating 1 and the determined peaks.

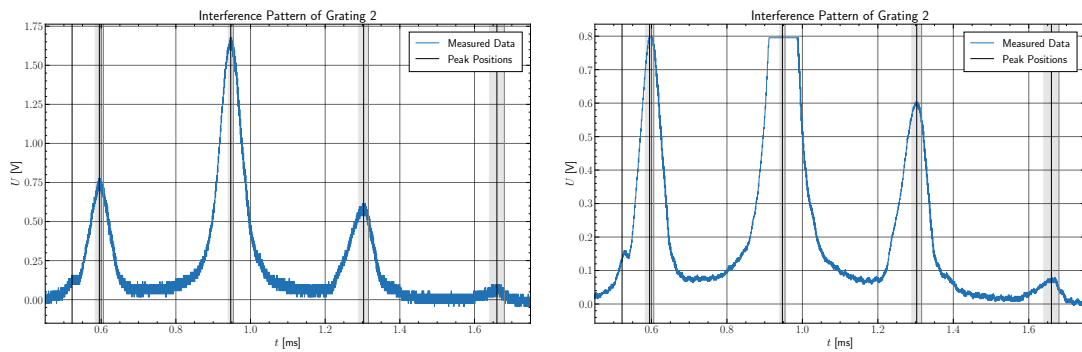


**Figure 18:** Interference Pattern for grating 2 and the determined peaks.

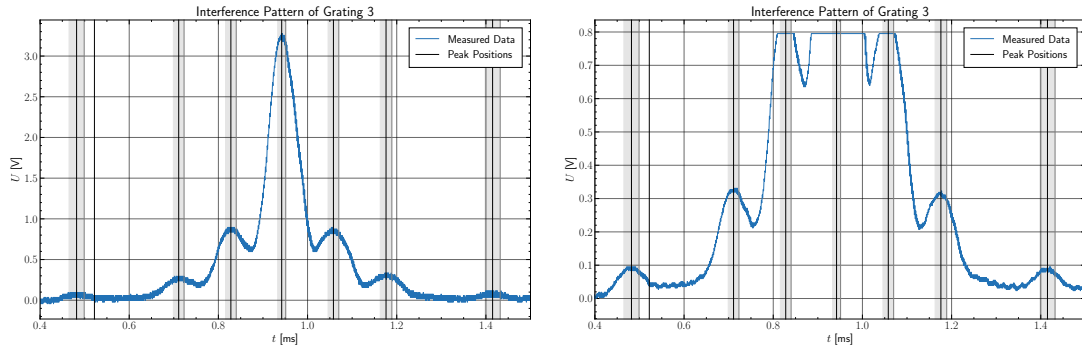


**Figure 19:** Interference Pattern for grating 3 and the determined peaks.

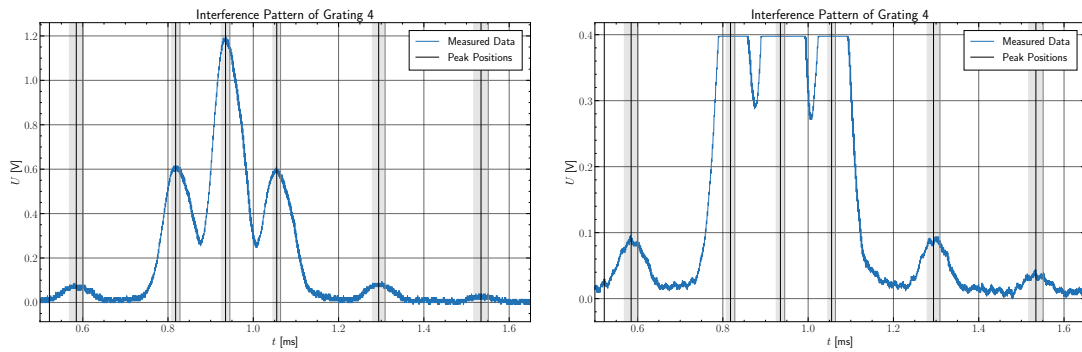


**Figure 20:** Interference Pattern for grating 4 and the determined peaks.

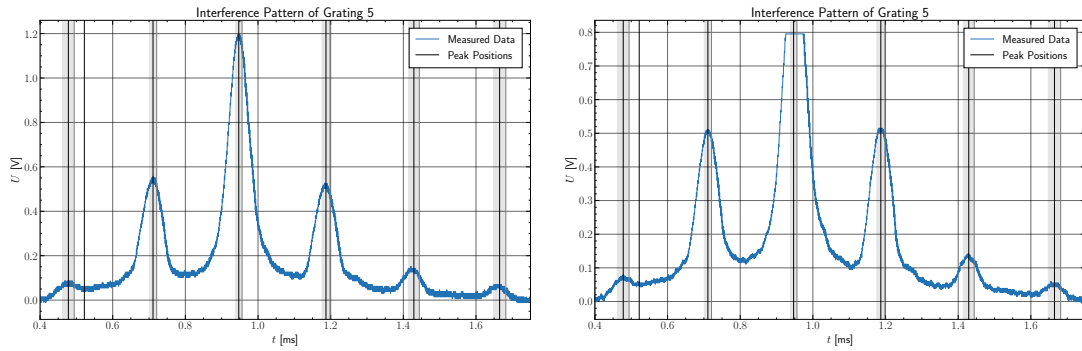


**Figure 21:** Interference Pattern for grating 5 and the determined peaks.

## A.2 Interference Pattern for the Ultrasonic Chamber at different Voltages

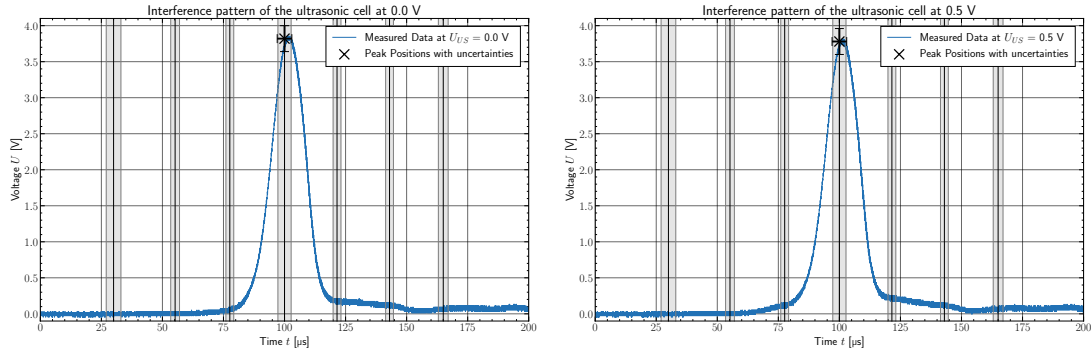


Figure 22: Interference Pattern for the Ultrasonic Chamber at 0.0 V and 0.5 V.

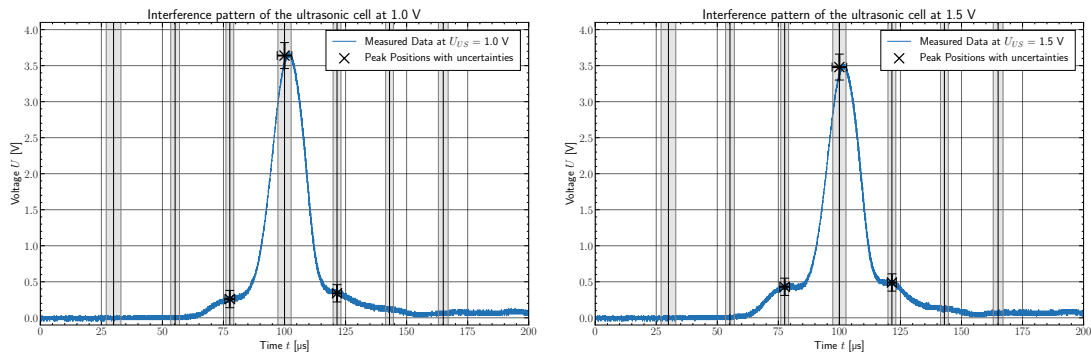


Figure 23: Interference Pattern for the Ultrasonic Chamber at 1.0 V and 1.5 V.

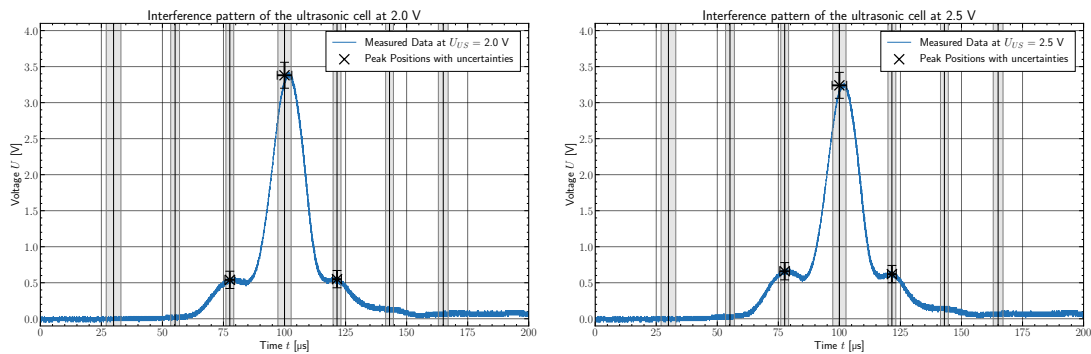


Figure 24: Interference Pattern for the Ultrasonic Chamber at 2.0 V and 2.5 V.

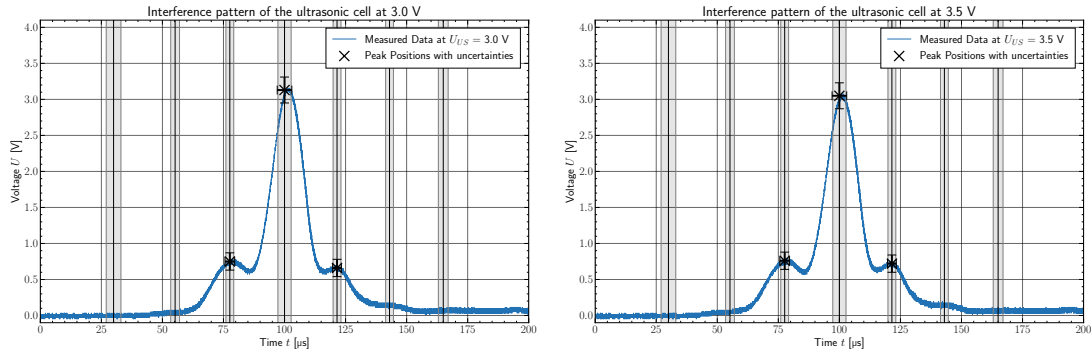


Figure 25: Interference Pattern for the Ultrasonic Chamber at 3.0 V and 3.5 V.

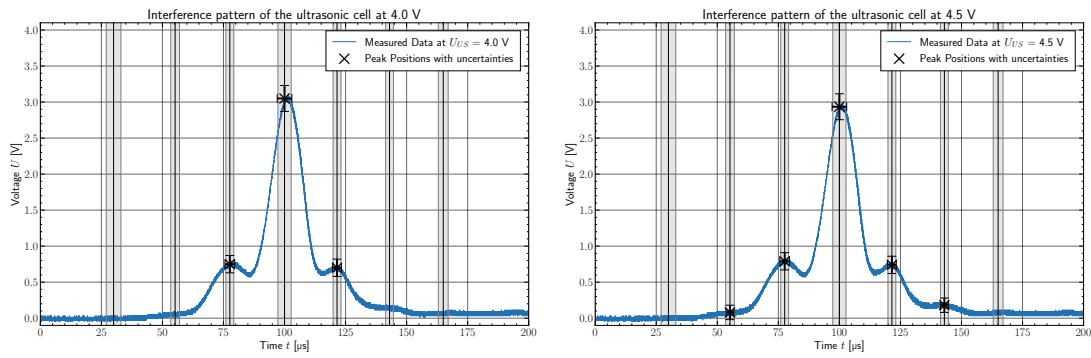


Figure 26: Interference Pattern for the Ultrasonic Chamber at 4.0 V and 4.5 V.

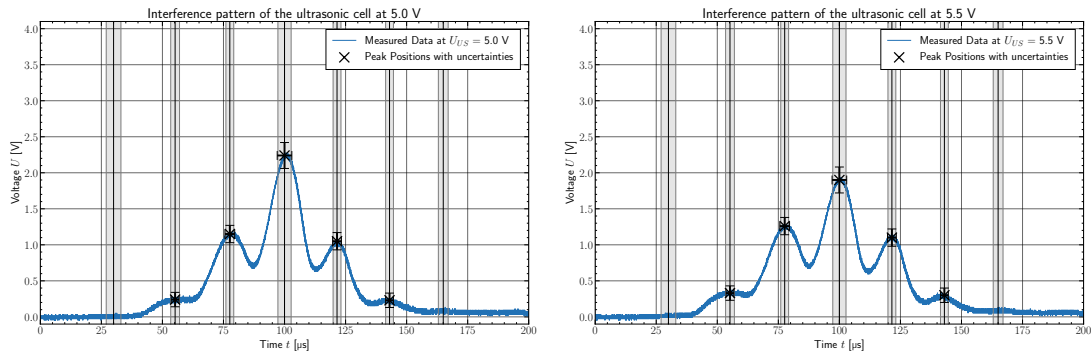


Figure 27: Interference Pattern for the Ultrasonic Chamber at 5.0 V and 5.5 V.

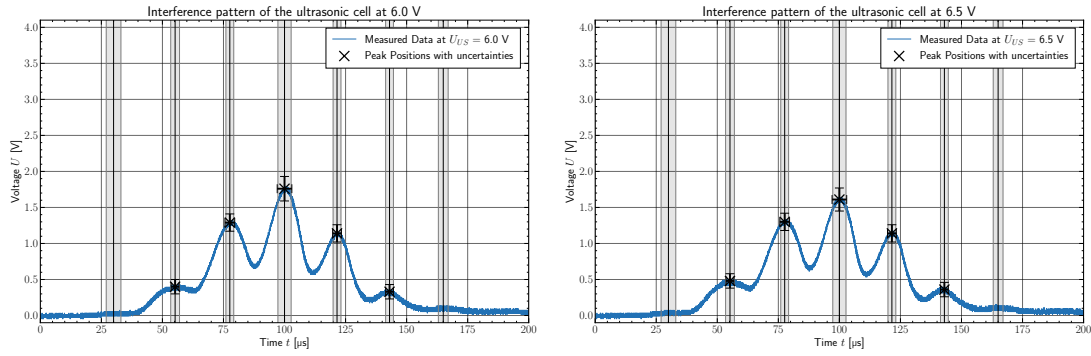


Figure 28: Interference Pattern for the Ultrasonic Chamber at 6.0 V and 6.5 V.

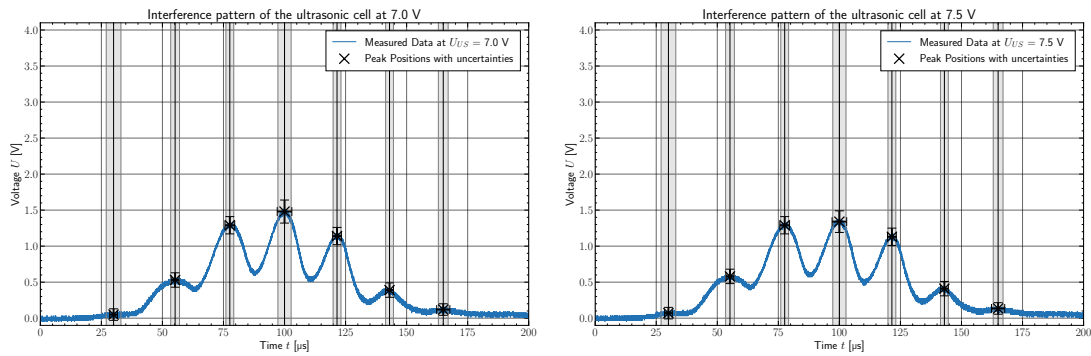


Figure 29: Interference Pattern for the Ultrasonic Chamber at 7.0 V and 7.5 V.

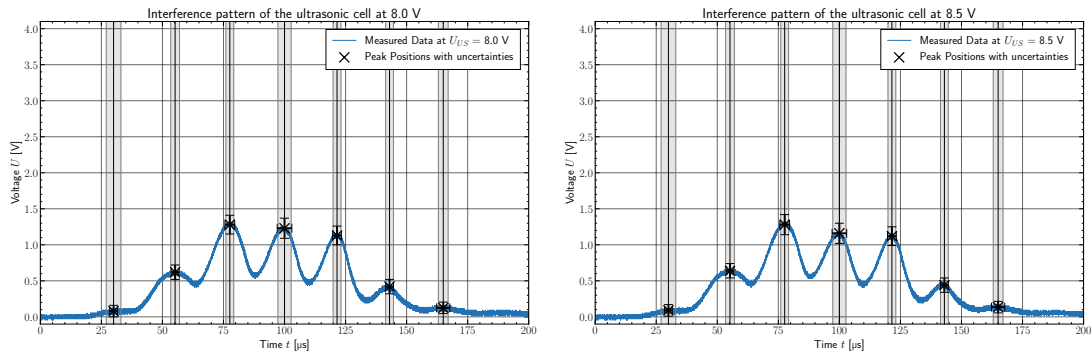
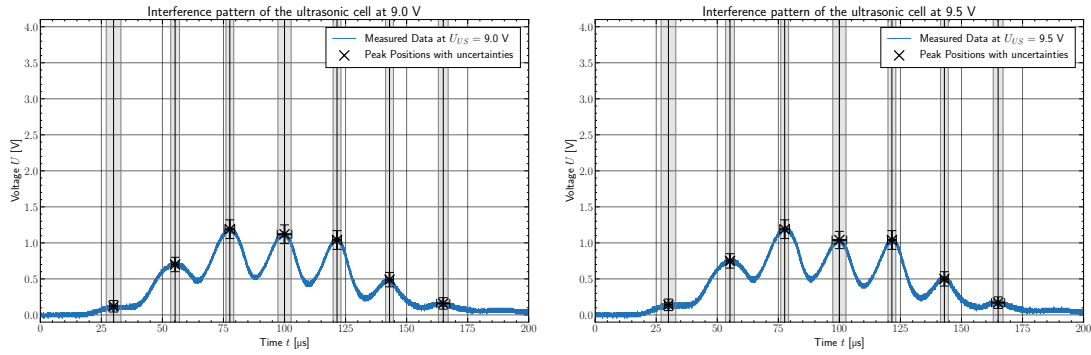
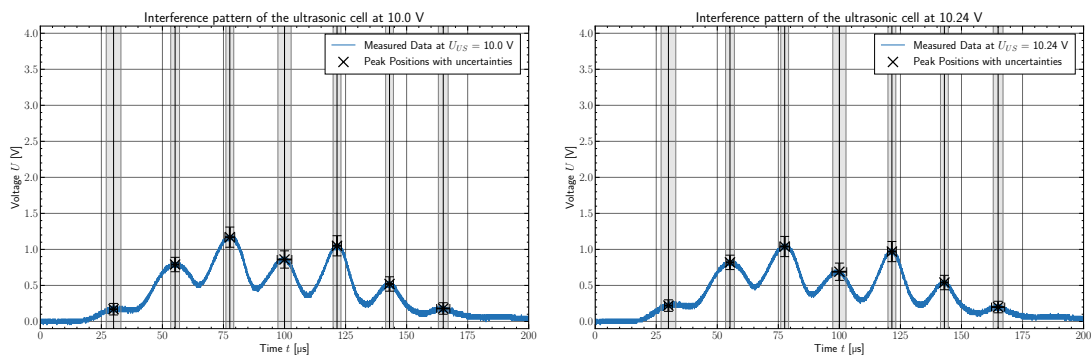


Figure 30: Interference Pattern for the Ultrasonic Chamber at 8.0 V and 8.5 V.



**Figure 31:** Interference Pattern for the Ultrasonic Chamber at 9.0 V and 9.5 V.



**Figure 32:** Interference Pattern for the Ultrasonic Chamber at 10.0 V and 10.24 V.

A.3 Lab Notes

Ultraschall 07.09.22 - 08.09.22

Sine grid : distance measurement with lower ~~cell~~ 1/2 and rise

distance grid-screen  $(12,9 \pm 0,2)$  cm uncertainty estimated considering parallel error

maximum order 0  $(0,1 \pm 0,1)$  cm uncertainty estimated considering the width of the dot

max. of order 1 left  $(-5,3 \pm 0,1)$  cm

" right  $(+5,6 \pm 0,1)$  cm

5 different grids

measurement	angle offset
reference	$(30 \pm 5)^\circ$
grating 1	$(20 \pm 5)^\circ$
grating 2	$(20 \pm 5)^\circ$
grating 3	$(20 \pm 5)^\circ$
grating 4	$(20 \pm 5)^\circ$
grating 5	$(20 \pm 5)^\circ$

5 different grids

width of light : ~~3mm~~  $(3,0 \pm 0,5)$  mm

frequency : ~~2496,324~~ kHz  
 error : ~~0,05~~ kHz  
 voltage error : 0,01 V

frequency  $(2284,873 \pm 0,5)$  kHz } measurement 1  
 reference grating angle :  $(15 \pm 5)^\circ$

$(2302,222 \pm 0,5)$  kHz } measurement 2  
 $(20 \pm 5)^\circ$

$(2299,999 \pm 0,5)$  kHz } measurement 3  
 $(17 \pm 2)^\circ$

09.09.2022  
 [Signature]